Journal of Geochemical Exploration 182 (2017) 94–109

Contents lists available at ScienceDirect

Journal of Geochemical Exploration

journal homepage: www.elsevier.com/locate/gexplo

Origin of diagenetic calcite cements in the continental Qaidam Basin, NW China: Implication for fluid flow and hydrocarbon migration

Aiguo Wang[a,*], Ting Liang[b], Long Li[c], Zhenliang Wang[a], Changyu Fan[a], Yisong Wang[a], Yongshu Zhang[d], Hongxi Kong[d]

[a] State Key Laboratory of Continental Dynamics, Department of Geology, Northwest University, Xi'an, Shaanxi 710069, China
[b] College of Geosciences, China University of Petroleum, Beijing 102249, China
[c] Department of Earth and Atmospheric Sciences, University of Alberta, Edmonton, Alberta T6G 2E3, Canada
[d] Institute of Exploration and development, PetroChina Qinghai Oilfield Company, Dunhuang, Gansu 736202, China

ARTICLE INFO

Keywords:
Calcite cement
Continental basin
Fluid flow
Hydrocarbon migration
Qaidam Basin

ABSTRACT

Diagenetic carbonate cements have been widely investigated to reveal fluid information in marine basins. However, they have not been well studied in continental basins. This paper addresses this issue using a case study in the northern Qaidam Basin, northwest China. The calcite cements in the reservoir sandstones were investigated by an integrated analysis including petrology, mineralogy, carbon and oxygen isotopes and fluid inclusion. Calcite is the dominant cement and main cause of poor porosity in the sandstones. The $\delta^{13}C_{PDB}$ and $\delta^{18}O_{PDB}$ values of calcite cements display a wide isotopic range, varying from −13.5 to 2.5‰ and −16.7 to −4.7‰, respectively. However, the $\delta^{13}C_{PDB}$ and $\delta^{18}O_{PDB}$ values from the central basin are within a limited range (−4.2 to −2.0‰ and −11.2 to −9.4‰, respectively). Dull- and bright-luminescence zones and two populations of fluid inclusion indicate two generations of calcite (Ca 1 and Ca 2) in N1 well. Ca 1 and Ca 2 have similar $\delta^{13}C_{PDB}$ values (−8.7 to −7.0‰), whereas the $\delta^{18}O_{PDB}$ values (−13.7 to −13.1‰) of Ca 2 are more negative than those (−10.8 to −9.8‰) of Ca 1.

Three origins of calcite cement were clearly identified: (i) hydrocarbon source rocks in thermal degradation stage, (ii) lacustrine carbonates in deep strata, and (iii) paleo-lakewater. Two episodes of organic fluids derived from the Jurassic source rocks flowed towards the basin margin, resulting in two rounds of acidic → hydrocarbon → alkaline fluid evolution identified in the reservoir sandstones. Calcite (Ca 1) precipitation generated highly calcite-cemented sandstones, which severely downgraded the reservoir quality. However, the second episode of acidic fluid created new porous zones for subsequent hydrocarbon accumulation. Although the cementation history in the central basin did not occlude all porosity, the presence of fluids derived from buried lacustrine carbonates suggests a poor prospect for hydrocarbon migration. The good spatial correlation between the occurrence of the ^{13}C-depleted calcite cement and the presence of hydrocarbons suggests that the ^{13}C-depleted calcite (relative to lacustrine carbonates) may be an indicator of hydrocarbon migration in the northern Qaidam Basin.

1. Introduction

Many of major hydrocarbon-bearing basins in China are continental sedimentary basins. Understanding the properties and flow patterns of fluid within these basins is extremely important for hydrocarbon exploration and production. Diagenetic carbonate cements can provide valuable information on diagenetic and hydrocarbon fluids in sedimentary basins (e.g., Baker et al., 1995; Guo et al., 2013; Mozley and Wersin, 1992; Wang and Zhang, 2001). Numerous studies have been performed to examine the origin, timing, diagenetic environment and geochemical evolution of pore-water in reservoir rocks, by analyzing the variations in petrography, mineralogy, isotopic and elemental compositions of carbonate cements in the basins worldwide (e.g., Brigaud et al., 2009; Calvo et al., 2011; El-Ghali et al., 2013; Maliva, 1995; Mansour et al., 2014; Morad et al., 1996; Morad et al., 2000; Mozley and Hoernle, 1990; Odigi and Amajor, 2010; Qing et al., 2006; Xiong et al., 2016). However, the vast majority of carbonate cements in these studies were related to marine-derived pore water rather than lacustrine-derived. Unlike seawater, the geochemical compositions of lakewater are locally controlled and sometimes difficult to constrain.

* Corresponding author.
E-mail address: wag@nwu.edu.cn (A. Wang).

http://dx.doi.org/10.1016/j.gexplo.2017.09.002
Received 6 February 2017; Received in revised form 12 July 2017; Accepted 8 September 2017
Available online 12 September 2017
0375-6742/

The origins of carbonate cements in continental basins in previous studies, for example, were always roughly inferred based on their diagenetic stage (e.g., Wang et al., 2016) or reference to the isotopic compositions of normal seawater (e.g., Sun et al., 2010; Wang et al., 2007), which limited the geochemical investigation into fluid flow in continental basins.

The Qaidam Basin is a typical continental basin during the Cenozoic, in which continental depositions containing lacustrine carbonates (LC) are well persevered (Huang et al., 2016; Jian et al., 2014; Rieser et al., 2009; Zhao, 2015). Previous studies have showed that diagenesis did not significantly affect the isotope values of LC (Graham et al., 2005; Kent-Corson et al., 2009; Rieser et al., 2009). The isotopic compositions of the LC thus reflect the isotopic compositions of lakewater in which precipitation occurred (Deocampo, 2010). Moreover, carbonate cements have been reported to be the most prevalent cements in the sandstone reservoirs in the northern basin (e.g., Chen et al., 2012; Rieser et al., 2005; Sun et al., 2014; Wang and Wang, 2006; Wang et al., 2008; Zhang, 2010). So far, the knowledge of diagenetic fluid and hydrocarbon across the northern basin is still lacking, which has resulted in frequent exploration failure. Therefore, the northern Qaidam Basin provides an excellent opportunity to investigate origins of diagenetic carbonate cements and its application on fluid flow in a continental basin. The aim of this study is to (1) identify the origins of diagenetic calcite cements, (2) sketch the fluid flow across the basin, and (3) evaluate the impact of these fluid flows on reservoir quality and hydrocarbon migration.

2. Geological setting and sampling

Located in the northern Tibetan Plateau, the Qaidam Basin (Fig. 1a, b) is bounded by three major mountain ranges (Kunlun Mountains to the south, Altun Mountains to the northwest and Qilian Mountains to the northeast) and covers an area of 120,000 km^2 (Fan et al., 2014; Luo et al., 2013). The basin is composed of a Mesozoic-Cenozoic continental sedimentary cover (thickness of 3–17 km) on a basement consisting of Proterozoic-Lower Palaeozoic metamorphite and magmatite (Rieser et al., 2009; Xia et al., 2001; Yang et al., 2004). The Cenozoic structural evolution of the basin is closely linked with the continuous convergence between the Indian and Eurasian plates (Yin and Harrison, 2003; Yin et al., 2008), undergoing strike-slip basin, foreland basin and intermontane basin stages (Zhu et al., 2006). A series of thrust fold belts with NW–SE direction are present inside the basin (Fig. 1c). Reverse faults are developed along Qilian Mountains and Kunlun Mountains (Jian et al., 2014).

The study region is the Eboliang Anticline Belt (Fig. 1c), which is located in the northern basin (Fig. 1b). It consists of six NW-SE trending anticlines which, from northwest to southeast, are Eboliang I, Eboliang II, Hulushan, Eboliang III, Yahu and Yikeyawuru anticlines (Fig. 1c). These anticlines were developed at different time during the Pliocene (Fig. 2), with the oldest one along the basin margin and the youngest one in the central basin (Heermance et al., 2013; Yin et al., 2008). Decollement faults and fold structures were also produced in the Eboliang Anticline Belt due to lateral compression during the same period (Yin et al., 2008; Yang et al., 2004).

The sedimentary cover in the northern Qaidam Basin include the Middle-Lower Jurassic strata which are mostly fluvial and paludal depositions (Jian et al., 2013; Luo et al., 2013), and the Cenozoic strata that unconformably overlie the Jurassic (Fig. 2). The Jurassic strata occur along the basin margin at relatively shallow depths, while the thickness of the Cenozoic strata in the basin is > 10,000 m (Qiu, 2002). The Jurassic strata consist of clastic rocks including conglomerate, sandstone, siltstone, mudstone and transitional rocks between them (Ritts, 1999; Wang and Wang, 2006). The content of detrital quartz, feldspar and lithic grains in the sandy rocks is 5–77%, 5–59% and 2–87%, respectively. The lithic grains consist of volcanic rocks, quartzite, siltstone, mudstone and few carbonate grains (Wang and Wang, 2006). The lower Jurassic mudstones with dark coal measures (J_{1-2}d, Fig. 1c) are the likely source rocks of the Lower Jurassic–Lower Jurassic/Cenozoic petroleum system in the west section of the northern Qaidam Basin (Yang et al., 2004). These rocks are characterized by Type III–II kerogen, average TOC contents of 4%, and a wide range of thermal maturity, from immature to highly mature (Ritts, 1999; Wang et al., 2015).

The Cenozoic strata are composed of mixed evaporite–carbonate–siliciclastic deposits (Jian et al., 2013; Liu et al., 1998). The paleolake in the basin expanded continuously during the Paleogene, reached the largest surface during the subsidence stage of Upper Ganchaigou Formation (N_1g), and gradually shrank after that (Li et al., 2012; Yuan et al., 2015), leading to alluvial, fluvial, delta and lacustrine depositions in the basin (Jian et al., 2013; Zhang, 2010). The depocenter was located in the western Qaidam Basin during the Paleogene (Zhao, 2015), then migrated to the Yiliping area during the Miocene-Pliocene (Fig. 1c) (Chen et al., 2017; Zhao, 2015). As the paleolake was a saline lake during this geological period (Huang et al., 2016; Jian et al., 2013; Rieser et al., 2009; Zhao, 2015), the Cenozoic rocks consist of clastic rocks and LC. LC are intercalated in mudstones of the Lower Ganchaigou (E_3g) through the Upper Youshashan (N_2^2y) formations (Figs. 1b, 2), including micrite, bioclastic limestone, algal limestone, dolomicrite, algal dolomite and so on (Huang et al., 2016; Zhang et al., 2004; Zhao, 2015). In the northern Qaidam Basin, LC are developed in the Yiliping Sag (e.g., H2 well), but not in other areas (Table 1).

In recent years, seven exploration wells have been drilled along the axis of the Eboliang Anticline Belt (Fig. 1). The N1 and EI2 wells, located near the basin margin, extend into the Jurassic formation, whereas the other wells (E7, ES1, ES2, YC3 and YS1) penetrate only to the Neogene strata. Of these wells, only Well N1 has produced commercial oil and gas.

3. Analytical methods

3.1. Sample preparation and characterization

In total, 22 core samples from the seven wells above (Fig. 1) were selected for detailed petrographic and geochemical examination. To supplement the core samples from relatively deep strata, a sandstone outcrop located near basin margin was collected and examined as well.

The samples were impregnated with red epoxy to facilitate porosity recognition and then cut to make thin sections. Alizarin Red S and K-ferricyanide staining was further applied on the thin sections for carbonate mineral determination. Diagenetic features, detrital composition (%), cement content (%) and surface pore (%) were examined using an Olympus BX51 polarizing microscope. The thin sections containing any unrecognizable diagenetic minerals after above operations were subsequently sputter coated with gold, and further examined by a FEI Quanta 400 FEG scanning electron microcopy (SEM). SEM was equipped with back-scattered electron imaging (BSEI) and energy-dispersive X-ray (EDX).

Doubly-polished thick sections were prepared for ultra-violet fluorescence petrography and fluid inclusion examination under the Olympus BX51 microscope fitted with a high-pressure mercury lamp (providing 365 ± 10 nm ultraviolet light). The thick sections containing calcite cements were selected for cathodoluminescence (CL) characterization on a BII CLF-1 CL stage. The operating voltages were 5–8 kV and gun current levels were 300–500 μA.

3.2. Stable isotope analysis

Carbon and oxygen isotopic compositions ($\delta^{13}C$ and $\delta^{18}O$) were examined at both whole-rock and sub-millimeter scales. Pore-filling calcite exhibiting no obvious CL-defined zones was selected for whole-rock isotope analysis. Calcite veins, if exist, were firstly removed from the samples prior the CO_2 gas was extracted following the procedures

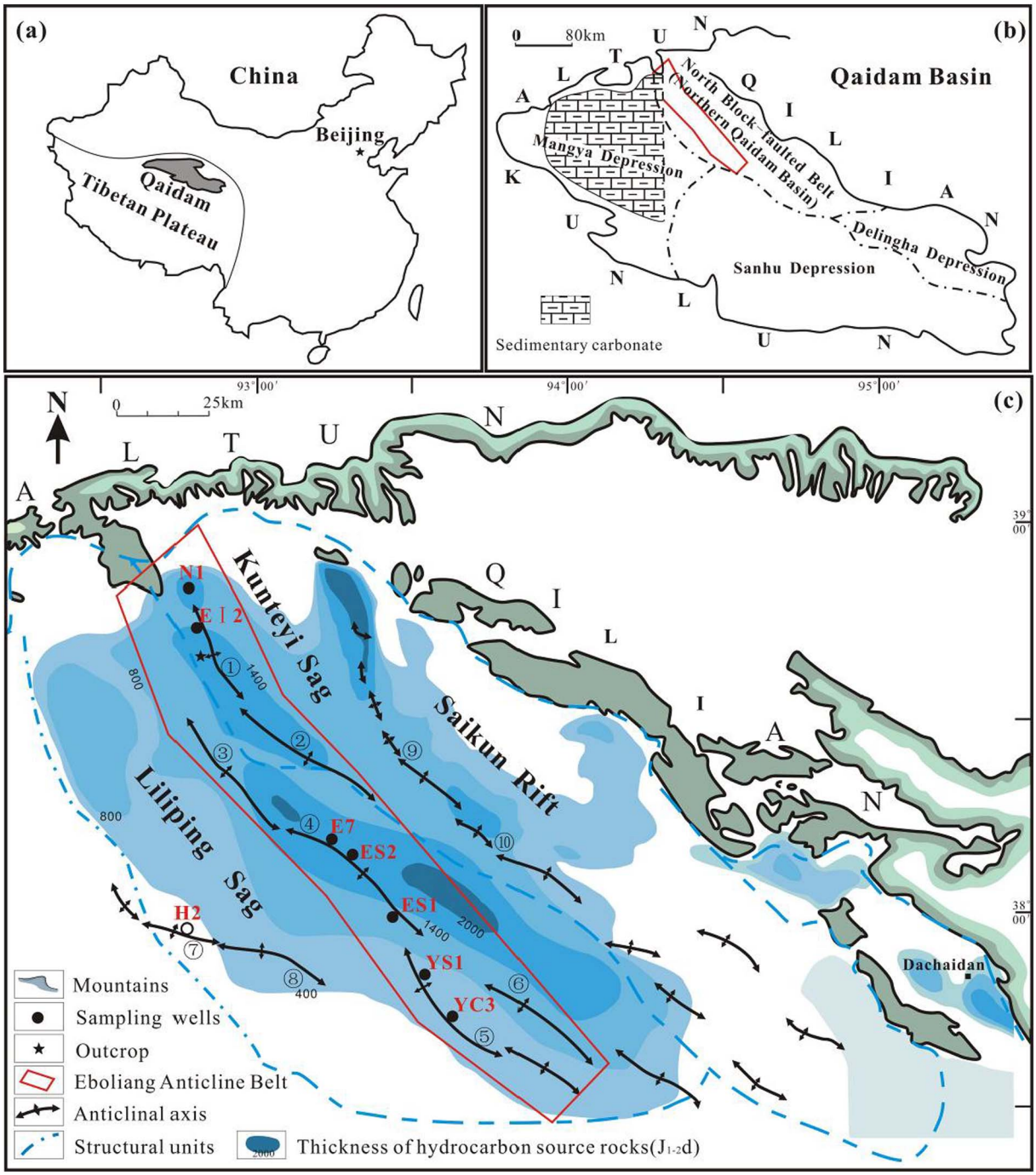

Fig. 1. Geographic location of the Qaidam Basin in China (a), tectonic units and lacustrine carbonate (Huang et al., 2016; Zhao, 2015; Zhang et al., 2004) in the Qaidam Basin (b), and location of the Eboliang Anticline Belt and sampling wells in the structural map of the northern Qaidam Basin (c). ①: Eboliang I anticline; ②: Hulushan anticline; ③: Eboliang II anticline; ④: Eboliang III anticline; ⑤: Yahu anticline; ⑥: Yikeyawuru anticline; ⑦: Hongsanhan III anticline; ⑧: Hongsanhan IV anticline; ⑨: Lenghu VI anticline; ⑩: Lenghu VII anticline.

described by McCrea (1950). Isotope ratios were measured using the Finnigan MAT-253 mass spectrometer. Calcite veins exhibiting well-defined CL-zones were selected for more detailed sub-millimeter isotope analysis. Calcite powders (10–50 μg) within each CL-defined zone were extracted using microdrilling techniques (Fouke and Rakovan, 2001). The extracted calcite powders were measured for carbon and oxygen isotopic compositions following the procedures described by Zhai et al. (2011) on a Finnigan MAT-253 mass spectrometer equipped with a Kiel IV carbonate preparation device. All the $\delta^{13}C$ and $\delta^{18}O$ data are reported in per mil (‰) relative to the V-PDB standard, and the analytical uncertainty (1σ) is better than 0.10‰ for $\delta^{13}C$ and 0.15‰ for $\delta^{18}O$.

3.3. Fluid inclusion analysis

Fluid inclusions were examined on a THMS600 Linkam Heating/Freezing stage for homogenization temperatures (Th) and final melting temperatures of ice (Tm). Heating rates were < 20 °C/min at beginning, but < 2 °C/min when approaching phase transition. The analytical uncertainties are better than 0.1 °C for both.

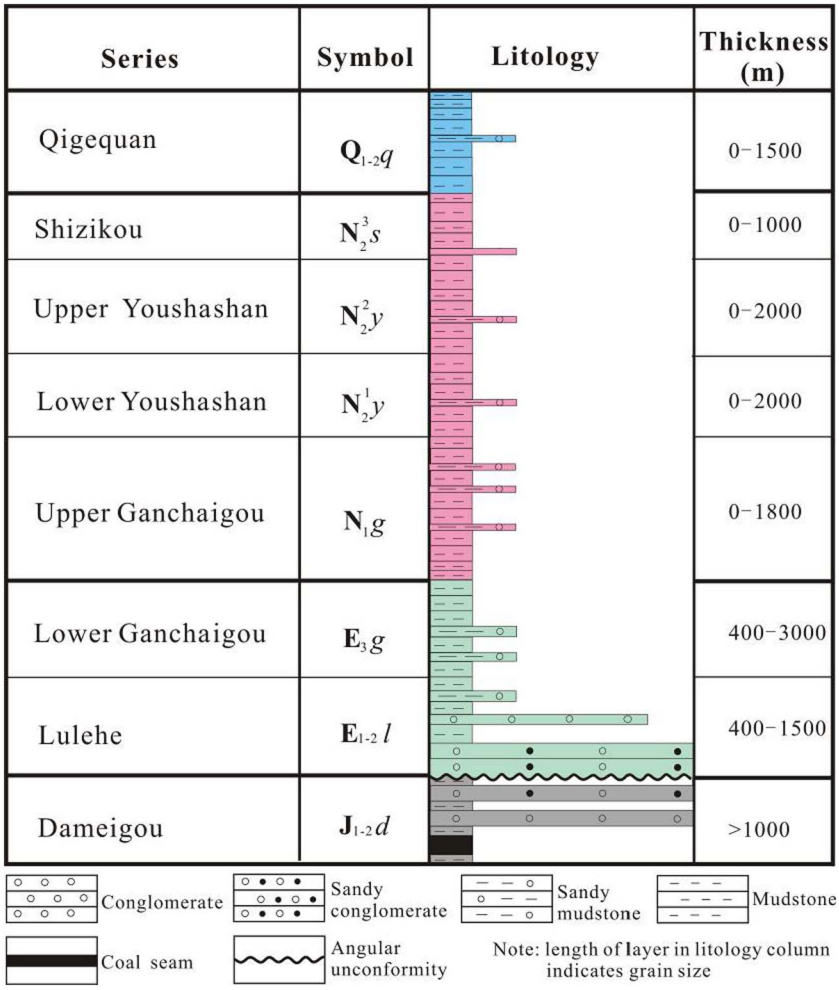

Fig. 2. Sketch showing the stratigraphic column and classification in the west section of the northern Qaidam Basin.

4. Results

4.1. Petrographic features of sandstones

Thin section examination indicates that the contents of quartz, feldspar and rock fragments are 7%–30% (av. 22%), 2%–47% (av. 22%) and 3%–62% (av. 33%). Based on Folk's (1980) sandstone classification scheme, the sandstones plot within the fields of arkose, lithic arkose, feldspathic litharenite and litharenite (Fig. 3). The detrital grains are fine- to very coarse-grained, angular to subrounded, presenting as point grain contact in the outcrop sample (Fig. 4A) and tangential grain contact (Fig. 4B–H) in the core samples. Overall, the sandstones in the basin are mainly fine-grained lithic arkose, whereas those along the basin margin are characterized by various grain sizes and sandstone types (Table 2, Fig. 3).

The lithic fragments are mainly of metamorphic origin, including quartzite (e.g., Fig. 4D), schist and slate in all samples. The igneous rock fragments account for up to 20% of rock volume in the Eboliang I anticline, but do not present in the Eboiang III-Yahu anticlines. Sedimentary rock fragments (< 4%) mainly present in the Eboiang III-Yahu anticlines, in which detrital carbonate content is < 2%. Moreover, clay matrix is developed in EI-2 well (up to 24%), but rare in other wells (< 2%).

The porosity varies from 0 to 20% (Table 2). Poor porosity mainly results from calcite cementation (Fig. 4, Table 2), while high porosity originates from well-preserved primary intergranular porosity (e.g., Fig. 4B) or dissolution of cements, grains and matrix (e.g., Fig. 4E, H).

Table 1
Lacustrine carbonates (LC) in the representative wells in the northern Qaidam Basin.

Anticline	Well	Drilling depth (m)	Drilled formation	Lithology of LC	Total thickness of LC (m)	Thickness percent of LC in well (%)	Formation of LC	Location of samples
Hongsanhan III	H2	6018	N_1g	Limestone, marlstone, calcareous mudstone	1630	27.09	N_1g, N_2^1y, N_2^2y	
Eboliang III	ES1	4908	N_1g	Calcareous mudstone	6	0.12	N_2^2y	N_2^1y, N_2^2y
	ES2	3698	N_1g	Calcareous mudstone	3	0.08	N_2^1y	N_1g
	E7	2649	N_2^1y	Marlstone	2	0.08	N_2^2y	N_2^1y
Yahu	YC3	5204	N_1g	Marlstone	29	0.56	N_2^1y, N_2^2y	N_1g, N_2^1y
Lenghu VII	LQ1	3950	E_3g	Calcareous mudstone	6	0.15	E_3g	
	LQ2	5000	E_3g		0	0.00		
Lenghu VI	LL1	5305	$E_{1+2}l$	Calcareous mudstone	2	0.04	N_2^1y	

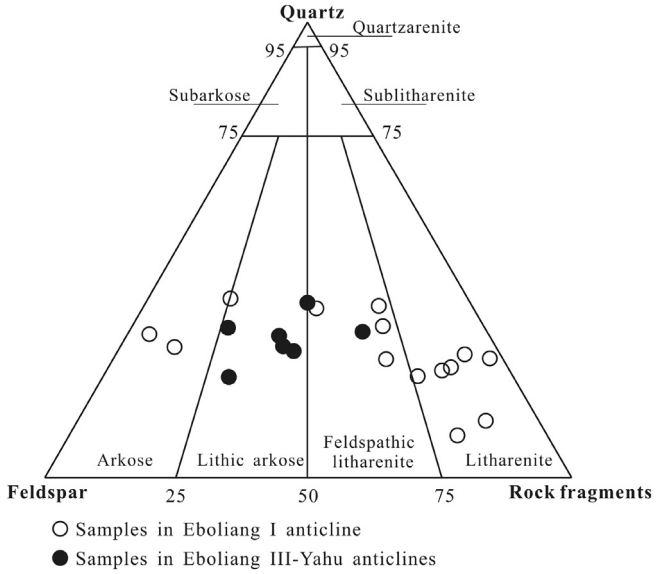

Fig. 3. Quartz–feldspar–rock fragments triangular diagram of sandstone petrography showing the composition of sandstones from the Eboliang Anticline Belt (Folk, 1980).

4.2. Calcite cement

Calcite that commonly occludes pores and fractures (Figs. 4, 5) in sandstones is the dominant cement, constituting up to 25% of rock volume (Table 2). The crystal size of fracture-filling calcite is larger than 1 mm (Fig. 5C–D), whereas that of pore-filling calcite is smaller than 0.03 mm (outcrop sample; Fig. 4A) or vary from 0.1 to 0.8 mm (core samples; Fig. 4). Quartzite grains, ferroan dolomite cement, kaolinite cement or sandstone matrix were partially replaced by the calcite in some core samples (e.g., Fig. 4C, D and G).

Pore-filling calcite exhibits non/dull or bright CL without identifiable growth zones (e.g., Fig. 5A–B). However, fracture-filling calcite (Sample 8) exhibited two CL-defined zones, including a dull-luminescence marginal zone (Ca 1) and a bright-luminescence central zone (Ca 2) (Fig. 5E–F). Thus, two generations of calcite were revealed, and the Ca 1 predates the Ca 2.

Aqueous fluid inclusions were studied in some of the calcite veins (Fig. 6A–B; Table 3). The inclusions are two-phase liquid-rich, showing filling ratio higher than 0.8 (e.g., Fig. 6B). Relatively large (> 5 μm) and well-preserved inclusions were measured for Th and Tm. The obtained Th values vary from 77.1 to 162.4 °C (Table 3), suggesting two inclusion populations (Fig. 7). The first one, corresponding to formation of Ca 1, homogenizes at 80–100 °C, while the other one, corresponding to Ca 2 formation, homogenizes at 120–150 °C. The Tm values vary from − 2.0 to − 5.1 °C (Table 3) without clear separation of the two populations.

4.3. Other cements

Authigenic kaolinite is common in the Jurassic sandstones of the N1 well, but rare in other wells. It occurs in intergranular pores as flaky kaolinite aggregate, constituting up to 7% of rock volume (Table 2). Amorphism in SEM and strong carbon signal in EDX (Fig. 4G, H) suggest that the kaolinite aggregate has been stained by bitumen.

Pyrite (< 1.6%) occurs in the Eboliang I anticline, while quartz cement (< 0.2%) and ferroan dolomite (< 1%) are present in the Eboliang III-Yahu anticlines (Table 2). Pyrite formed earlier than calcite. Quartz cement occurs as overgrowth on some detrital quartz grains. Anhydrite (up to 9%) was found only in the limited sandstones of the YC3 well (Table 2).

4.4. Hydrocarbons

Oil inclusions (e.g. Fig. 6C–D) and bitumen (e.g. Fig. 4F) exhibiting yellow and bluish-white fluorescence were observed in the sandstones from the Eboliang I anticline. Oil inclusions were trapped within secondary healed fractures in quartz, and no coexisting aqueous inclusions were found in this study. The yellow fluorescing oil inclusions homogenize at 51.2–59.4 °C, while the bluish-white ones homogenize at 82.8–128.5 °C which obviously exceed the highest paleogeothermal temperature (25 °C) experienced by the formation. In the secondary pore created by the dissolution of calcite and feldspathic/lithic grains, the bluish-white fluorescing bitumen (Hy 2) occupied the pore, while the yellow fluorescing bitumen (Hy 1) filled the nearby sandstone throats (Fig. 4E–F). Notably, bitumen and oil inclusions were not observed in the sandstones from the Eboliang III-Yahu anticlines.

Commonly, the fluorescence of petroleum changes in an order of red — yellow — orange — blue — bluish white with increased maturity (Munz, 2001; Stasiuk and Snowdon, 1997). The yellow and bluish-white fluorescing bitumen and oil inclusion indicate at least two episodes of hydrocarbon filling, corresponding to Hy 1 and Hy 2, respectively.

4.5. Carbon and oxygen isotopes

As rare detrital carbonates and ferroan dolomite cement occurred in the sandstones, whole-rock isotope analysis was expected to reveal the carbon and oxygen isotopic compositions of pore-filling calcite cement. Furthermore, the pore-filling calcite exhibits no obvious CL-defined zones in one sample (Fig. 5A, B), indicating that the whole-rock isotopic data represent single generation of calcite (Ca 1 or Ca 2). This is further supported by clear separation of these two groups in the plot (Fig. 8).

Calcite cements show wide $\delta^{13}C$ and $\delta^{18}O$ ranges. The $\delta^{13}C$ values vary between − 13.5 and 2.5‰, while the $\delta^{18}O$ values vary between − 16.7 and − 4.7‰ (Fig. 8). However, the $\delta^{13}C$ and $\delta^{18}O$ values of calcite cements from the Eboliang III-Yahu anticlines are within limited ranges (Fig. 8), varying from − 4.2 to − 2.0‰ and − 11.2 to − 9.4‰, respectively. In contrast, the calcite cement from the outcrop (Sample 14) shows similar $\delta^{13}C$ value (− 2.56‰) but higher $\delta^{18}O$ value (− 4.74‰), while the calcite cements from the basin margin are characterized by lower $\delta^{13}C$ values (− 13.5 to − 7.0‰) and more variable $\delta^{18}O$ values (− 16.7 to − 6.4‰).

Across the different luminescence zones of calcite vein in N1 well, the $\delta^{13}C$ values are relatively steady (− 8.7 to − 7.0‰), whereas the $\delta^{18}O$ values are more variable (− 13.7 to − 9.8‰). The $\delta^{18}O$ values of bright-luminescence zone are more negative than those of non-/dull-luminescence zone (Table 4; Fig. 5E–F). Overall, calcite cements in the Jurassic sandstone of N1 well can be divided into two classes based on the isotopic compositions, which correspond to Ca 1 and Ca 2, respectively (Fig. 8).

5. Discussion

5.1. Origin of calcite cement

Owing to rare presence of detrital carbonates in the northern basin, organic matter and lakewater are probably the organic and inorganic carbon sources, respectively. Organic matter is dispersed in fine-grained sedimentary rocks (e.g., shale) and is characterized by very negative $\delta^{13}C$ values, within the range between − 35‰ and − 20‰ (PDB) (Dutton and Land, 1985; Irwin et al., 1977). As lakewater can (1) directly precipitate calcite cement, (2) provide carbon for LC, and (3) be inevitably trapped in formation as pore water during burying, paleolakewater and its derivative (i.e., LC and buried pore water) are both the potential inorganic carbon sources of digenetic calcite cements. The reported $\delta^{13}C$ values of the well-preserved Cenozoic LC in the western basin (e.g., Rieser et al., 2009; Yin et al., 2007; Jian et al., 2014) vary

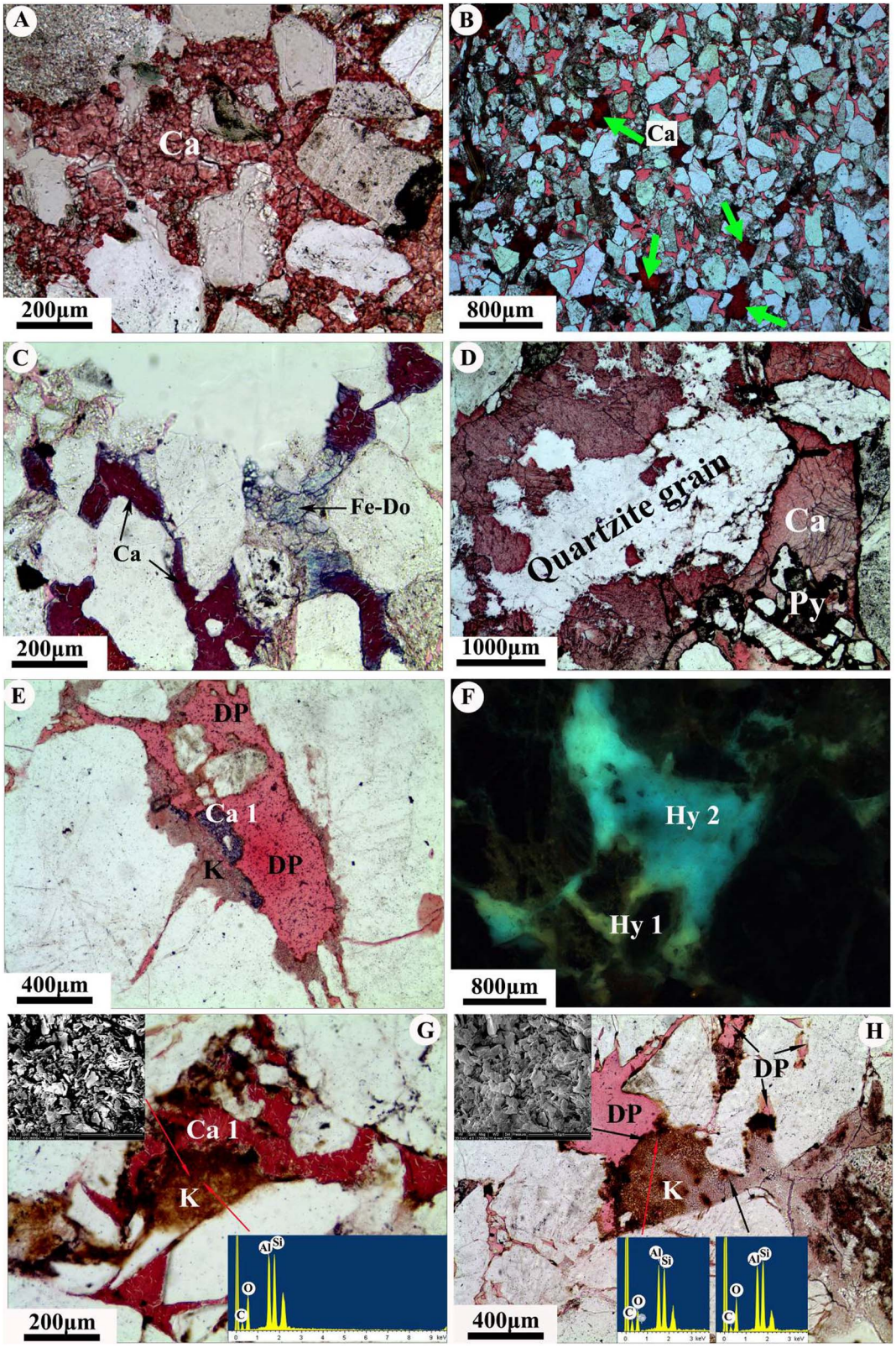

Fig. 4. Thin-section photomicrographs displaying occurrences of cements and bitumen in the reservoir sandstones from the Eboliang Anticline Belt. (A) Detrital grains appear as point contact, and microcrystalline calcite (Ca) completely occupied intergranular porosity, Outcrop. (B) Calcite (indicated by arrow) partially filled intergranular pore and considerable primary intergranular pore was saved, Well ES1, 1995.15 m. (C) Calcite occupied post-compaction pore and partially replaced ferroan dolomite (Fe-Do), Well ES2, 3032.73 m. (D) Calcite partially replaced quartzite grain and postdates pyrite (Py), Well EI2, 4048.78 m. (E–F) The first episode of calcite (Ca 1) postdated kaolinite (K). The dissolution of Ca 1 and detrital grains generated dissolution pore (DP), which was occupied by the bluish-white fluorescing bitumen (Hy 2). the yellow fluorescing bitumen (Hy 1) presented in the nearby sandstone throats, Well N1, 2229.72 m. (G–H) SEM shows that kaolinite was stained by bitumen. Subsequently, Ca 1 filled pore and probably replaced the bitumen-stained kaolinite. The intergranular pores nearby in this thin section were referred to originate from the dissolution of Ca 1 and detrital grains, Well N1, 2232.9 m. (For interpretation of the references to color in this figure legend, the reader is referred to the web version of this article.)

Table 2
Diagenetic cements, porosity and whole-rock stable isotopic compositions of carbonate cements in the sandstones from the Eboliang Anticline Belt.

Sample ID	Anticline	Well	Depth (m)	Formation symbol	Lithology	Authigenic cements (area %)						Porosity /%	$\delta^{13}C_{PDB}$/‰	$\delta^{18}O_{PDB}$/‰
						Calcite	Ferroan dolomite	Kaolinite	Anhydrite	Quartz overgrowth	Pyrite			
1	Eboliang I	N1	1162.8	E_3g	Fine sandstone	10.0					0.1	9.0	−7.43	−6.39
2	Eboliang I	N1	2225.37	$J_{1-2}d$	Very coarse sandstone			7.0				13.0		
3	Eboliang I	N1	2226.07	$J_{1-2}d$	Very coarse sandstone[a]	22.0		0.5			0.2	0.0	−8.40	−10.20
4	Eboliang I	N1	2226.97	$J_{1-2}d$	Coarse sandstone[a]	0.5		4.5				11.0		
5	Eboliang I	N1	2227.47	$J_{1-2}d$	Conglomerate	25.0					0.2	0.0	−9.30	−14.10
6	Eboliang I	N1	2229.72	$J_{1-2}d$	Coarse sandstone[a]	0.2		6.0			0.2	10.0		
7	Eboliang I	N1	2230.97	$J_{1-2}d$	Conglomerate	20.0		2.0			1.0	1.0	−7.40	−10.90
8	Eboliang I	N1	2232.57	$J_{1-2}d$	Medium sandtone[a]	22.0		2.0			1.0	0.5	−9.4	−11.12
9	Eboliang I	N1	2232.9	$J_{1-2}d$	Fine sandstone	3.0		5.0				4.0		
10	Eboliang I	EI2	4048.78	E_{1-2l}	Very coarse sandstone	18.0					1.6	0.4	2.54	−7.18
11	Eboliang I	EI2	4645.36	$J_{1-2}d$	Fine sandstone	2.0						0.0	−8.50	−16.70
12	Eboliang I	EI2	4838.74	$J_{1-2}d$	Medium sandtone	18.0					0.3	0.0	−13.47	−15.93
13	Eboliang I	EI2	4842.12	$J_{1-2}d$	Medium sandtone	7.0						0.0	−11.30	−16.50
14	EboliangI	Outcrop	0	N_2^1y	Fine sandstone	25.0						0.0	−2.56	−4.74
15	Eboliang III	E7	1445.27	N_2^1y	Fine sandstone	5.0	1.0					20.0	−3.58	−9.59
16	Eboliang III	ES1	1995.15	N_2^1y	Fine sandstone	8.0						19.0	−3.15	−9.41
17	Eboliang III	ES1	3991	N_2^1y	Fine sandstone	6.0				0.2		10.0	−1.99	−10.95
18	Eboliang III	ES2	3032.73	N_1g	Fine sandstone	12.0	1.0			0.1		7.0	−4.24	−10.71
19	Yahu	YC3	4048.31	N_2^1y	Fine sandstone	5.0	0.5		9.0	0.2		3.5	−2.05	−10.32
20	Yahu	YC3	4918.04	N_1g	Fine sandstone	12.0	0.1					0.0	−3.10	−11.00
21	Yahu	YC3	4918.24	N_1g	Very fine sandstone	15.0	0.2		0.2	0.1		0.0	−3.8	−11.17
22	Yahu	YS1	2710.64	N_2^1y	Fine sandstone	5.0	1.0					8.0	−2.70	−10.20
23	Eboliang III	ES1	3621.2	N_2^1y	Calcareous mudstone							0.0	−4.11	−7.78

[a] Indicate core sample that contain calcite vein.

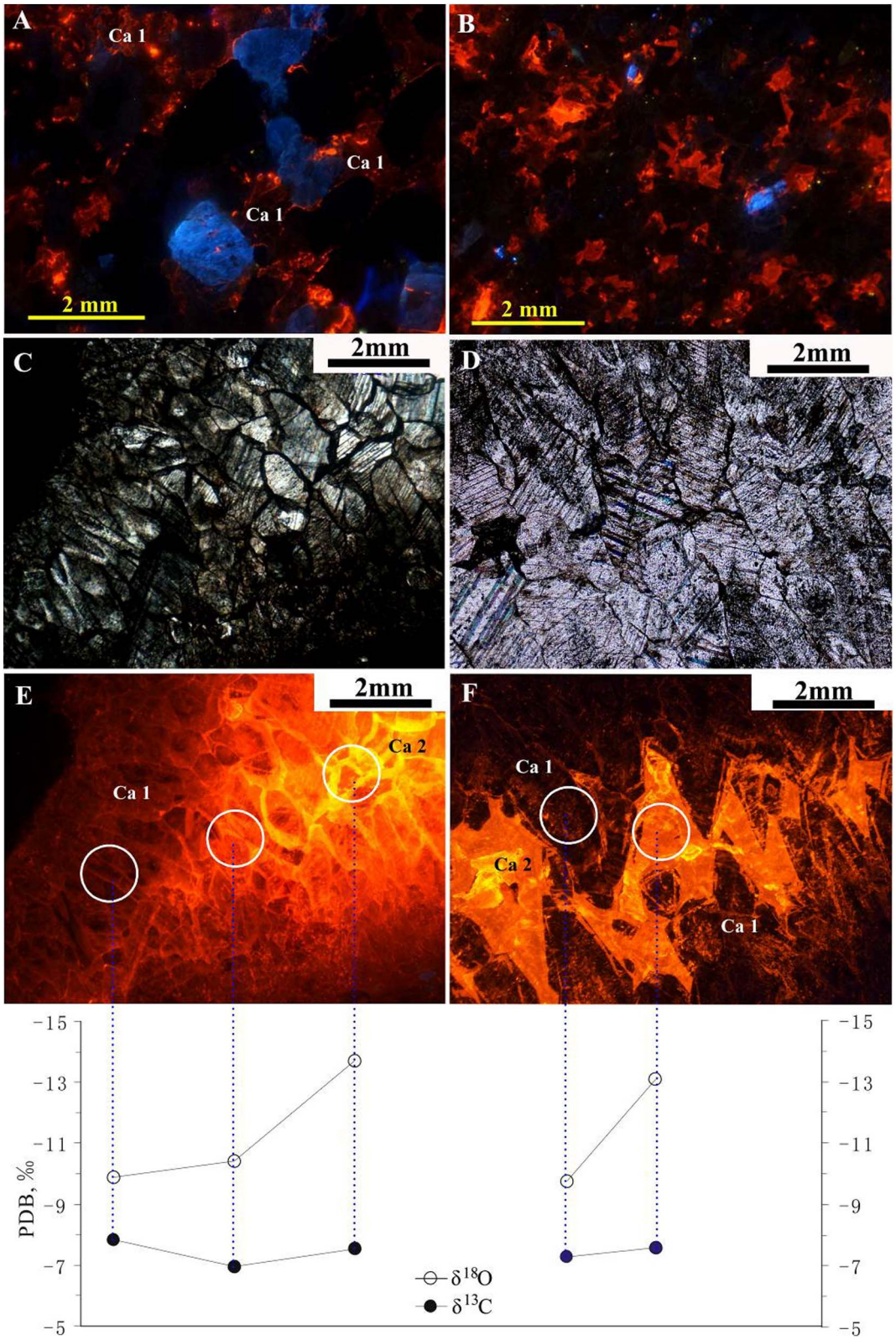

Fig. 5. Cathodoluminescence (CL) characteristics of calcite cements and the isotopic compositions of two CL-defined zones. (A) Pore-filling Ca 1 mainly exhibits non-luminescence, Well N1, 2232.57 m, (B) Pore-filling calcite exhibits uniform dull-luminescence, Well ES2, 3032.73 m. (C, D respectively match to E, F) Calcite vein exhibits two CL-defined zones: a dull-luminescence periphery (Ca 1) and a bright-luminescence nucleus (Ca 2). $\delta^{13}C$ values of the two calcite zones are relatively steady, whereas the $\delta^{18}O$ values vary widely. Well N1, 2232.57 m.

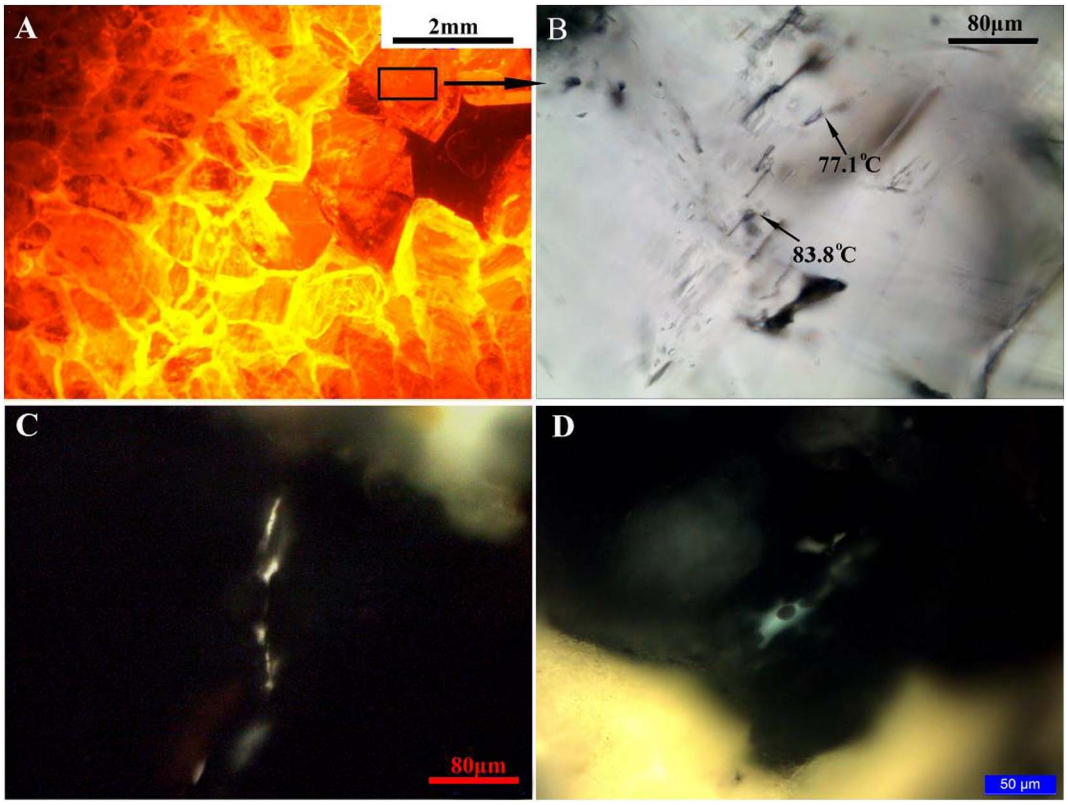

Fig. 6. Photomicrographs of fluid inclusions in the sandstones. (A–B) Primary aqueous inclusions were trapped in the dull-luminescence calcite vein, Well N1, 2232.57 m. (C) Yellow-white fluorescing oil inclusions were trapped in the secondary healed fracture in quartz, Well N1, 2232.9 m. (D) Bluish-white fluorescing oil inclusions were trapped in the secondary healed fracture in quartz, Outcrop. (For interpretation of the references to color in this figure legend, the reader is referred to the web version of this article.)

Table 3
Homogenization temperatures (Th) and final melting temperatures (Tm) of aqueous inclusions in calcite veins.

Sample ID	Depth(m)	Growth zones	Th (°C)	Tm(°C)
6	2229.72	Non-luminescence	88.5	− 4.9
		Bright-luminescence	135.8	− 2.8
		Dull-luminescence	129.7	–
		Dull-luminescence	127.3	− 4.6
		Dull-luminescence	85.3	–
7	2230.97	Non-luminescence	136.5	− 3.7
		Non-luminescence	118.9	–
		Bright-luminescence	147.5	–
		Dull-luminescence	115.6	− 2.2
		Non-luminescence	108.4	–
		Bright-luminescence	127.5	− 3.6
		Non-luminescence	92.7	–
8	2232.57	Dull-luminescence	83.8	− 2.0
		Dull-luminescence	77.1	–
		Bright-luminescence	148.1	− 3.9
		Bright-luminescence	151.6	− 4.7
		Bright-luminescence	162.4	− 5.1
		Bright-luminescence	159.3	–
		Dull-luminescence	93.2	–
		Dull-luminescence	124.1	− 4.3
		Bright-luminescence	137.3	–
		Bright-luminescence	142.8	− 3.8

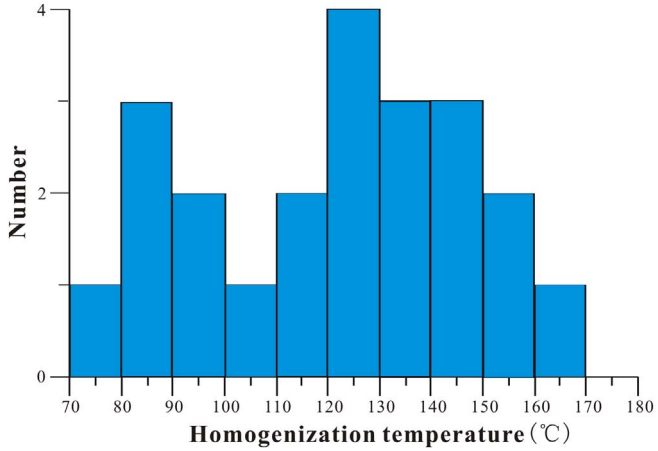

Fig. 7. Th histogram for the aqueous inclusions in calcite veins in the 2229.72–2232.57 m section of the Well N1. Two maxima of Th data correspond to two populations/episodes of diagenetic fluid, which precipitated Ca 1 and Ca 2 calcite.

from − 5.5 to 1.2‰, while the $\delta^{18}O$ values vary from − 8.4 to − 2.7‰ (Fig. 8). The $\delta^{13}C$ range of the LC likely represents that of the Cenozoic lakewater in the basin, due to slight fractionation of carbon isotope between LC and lakewater (Deocampo, 2010).

Compared to the LC, the calcite cement shows a wide range of isotopic compositions and can be clearly divided into two groups (Fig. 8). Group A showing lower $\delta^{13}C$ values than LC corresponds to the calcite cements (except Sample 14) from the basin margin. Group B showing similar $\delta^{13}C$ range and lower $\delta^{18}O$ values relative to the LC represents calcite cements from the central basin. Notably, the outcrop calcite cement (Sample 14) shows the same isotopic compositions as the LC.

5.1.1. Group A

Considering the hydrocarbon migration in the study area and degradation of the organic matter in the source-rock-region, it is reasonable to attribute the negative $\delta^{13}C$ values of Group A calcites to thermal degradation of organic matter (e.g. Irwin et al., 1977; Mansurbeg et al., 2012; Teichert et al., 2014; Wang, 2000). Given the facts that (1) calcite cements postdate hydrocarbon migration (Fig. 4G), and (2) Th values in

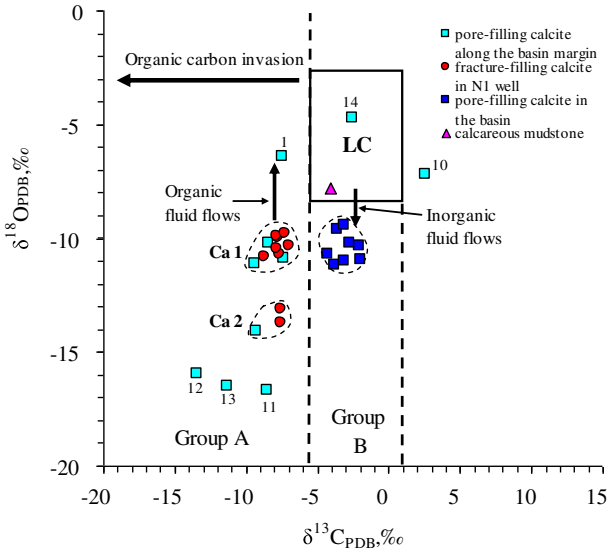

Fig. 8. Scatter diagram of $\delta^{13}C$ vs. δ^{18} O values for the calcite cements. Arabic numbers represent the sample ID. The rectangle represents the isotopic range of well-preserved Cenozoic lacustrine carbonates (LC) in the Qaidam Basin (Rieser et al., 2009; Yin et al., 2007; Jian et al., 2014). Compared with LC, the calcite cements can be divided into two groups. Group A has $\delta^{13}C$ values lower than LC. Different episodes (indicated by Ca 1 and Ca 2) and precipitating depths caused $\delta^{18}O$ variation. Group B has the similar $\delta^{13}C$ range as LC, but lower $\delta^{18}O$ values than LC.

the calcite veins are higher than 77.1 °C, Group A calcites likely resulted from invasion of fluids that dissociated CO_2 produced by the thermal degradation of organic matter within the Jurassic source rocks. Many factors, e.g. isotopically heterogeneous source rocks or variable mixing ratios between the organic and the inorganic carbon, can cause $\delta^{13}C$ variation of the fluid and the calcite. However, both generations of calcite cement (Ca1 and Ca2) in the N1 well show narrow range of $\delta^{13}C_{calcite}$ (−9.4 to −7.0‰; Fig. 8), suggesting isotopically homogeneous carbon source. Relatively stable Tm values of aqueous fluid inclusions (Table 3) point to the absence of significant fluid mixing. In such a case, the large $\delta^{18}O$ range (−14.1 to −6.4‰) of theses calcites indicates variable precipitating temperatures (Ankertell and Mriheel, 2000; O'Neil et al., 1969; Wang, 2000) which were caused by two major factors: (1) depth of calcite formation and local geothermal gradient, and (2) different episodes of precipitating fluids originated from the Jurassic source rocks.

As Ca 1 and Ca 2 are located within the narrow depth section (2225.37–2232.9 m), the $\delta^{18}O$ difference between them must be attributed to the factor (2). For $\delta^{18}O$ variation within a large depth range, both factor (1) and (2) should be considered. In the N1 well, the $\delta^{18}O$ value of Sample 1 is 4.03‰ and 7.24‰ higher than those of Ca 1 and Ca 2 respectively, while the depth is approximate 1070 m shallower than those. In order to determine the cause, we firstly assessed the isotope composition of the fluids corresponding to Ca 1 and Ca 2 precipitation (referred to as PF 1 and PF 2 fluids, respectively). Assuming

Table 5
Estimated $\delta^{18}O$ values of fluids precipitating Ca 1 and Ca 2 calcites.

Generation	$\delta^{18}O_{calcite}$ (‰, PDB)	Precipitating temperature (°C)	$\delta^{18}O_{fluid}$ (‰, PDB)
PF1/Ca 1	−11.12 ~ −9.78	80–100	−30.5 ~ −26.9
PF2/Ca 2	−14.10 ~ −13.08	120–150	−29.2 ~ −25.7

that oxygen isotope fractionation reached equilibrium, the $\delta^{18}O$ values of PF 1 and PF 2 were calculated (Table 5) using the oxygen fractionation equation (O'Neil et al., 1969), fluid inclusion homogenization temperature (Th) and measured $\delta^{18}O$ values of Ca 1 and Ca 2. If both PF 1 and PF 2 had flowed upward and precipitated calcite at the depth corresponding to Sample 1, the expected $\delta^{18}O$ values of calcite would respectively be −10.2 to −3.6‰ and −14.3 to −7.8‰, based on the geothermal gradient (3.0–2.1 °C/100 m) during the Cenozoic (Qiu, 2002; Zeng, 2009). Since the measured $\delta^{18}O$ value (−6.4‰ in Table 2) of Sample 1 better fit the modeled result of PF 1, the calcite cement in Sample 1 was likely precipitated from PF 1.

Furthermore, the $\delta^{18}O$ variation of calcite cement caused by the geothermal gradient suggests that the PF 1 fluid flowed slowly enough to reach equilibrium with the geothermal gradient. Thus, the main pathways for PF 1 are likely connected sandstone layers. As the precipitating temperatures of PF 2 (Fig. 7; Table 5)greatly exceed the highest paleogeothermal temperature (100 °C) experienced by the Jurassic formation at this depth, the main pathways for the PF 2 fluid are likely faults.

5.1.2. Group B

Group B calcites occur in the Neogene sandstones of the Eboliang III-Yahu anticlines. Their $\delta^{18}O$ values decrease steadily along depths (Fig. 9), which is apparently consistent with the geothermal gradient effect. However, the $\delta^{18}O$ difference between the deepest and the shallowest samples are expected to be 9.1–11.3‰ based on a geothermal gradient of 2.4–2.1 °C/100 m during the Pliocene and Quaternary (Qiu, 2002; Zeng, 2009). It is far larger than the measured $\delta^{18}O$ difference of 1.4–1.6‰ (see Fig. 9 and Table 2). This discrepancy may be explained by fast flow of the fluid along the vertical faults (Fig. 10). When a large amount of fluid flows upward rapidly, the fluid may not reach thermal equilibrium with the local host-rock. Consequently, the difference between precipitating temperatures at different depths is much smaller than expected, resulting in small variation in $\delta^{18}O$ values of calcite cements. This explanation is further supported by (1) calculations of Fan et al. (2016), who demonstrated that up to 57% of the total pressure in overpressured strata (> 2000 m) in the Eboliang III-Yahu anticlines was transferred through vertical faults and laterally conducting layers; and (2) aqueous inclusions, whose homogenization temperatures greatly exceed the highest formation temperature, occurred in the reservoirs of the Eboliang III-Yahu anticlines (Fan et al., 2016).

The $\delta^{13}C$ range of Group B calcites is similar to LC, suggesting an inorganic lakewater-origin carbon. However, Group B calcites were not

Table 4
Stable isotopic compositions obtained from the CL-defined zones of calcite veins.

Sample ID	Depth(m)	Formation	Luminescence	$\delta^{13}C_{PDB}$/‰	$\delta^{18}O_{PDB}$/‰
3	2226.07	$J_{1-2}d$	Non-luminescence	−7.62	−10.68
6	2229.72	$J_{1-2}d$	Non-luminescence	−7.74	−9.97
			Dull-luminescence	−8.70	−10.84
			Non-luminescence	−7.88	−10.47
8	2232.57	$J_{1-2}d$	Non-luminescence	−7.83	−9.89
			Dull-luminescence	−6.97	−10.35
			Bright-luminescence	−7.52	−13.71
			Non-luminescence	−7.26	−9.78
			Bright-luminescence	−7.60	−13.08

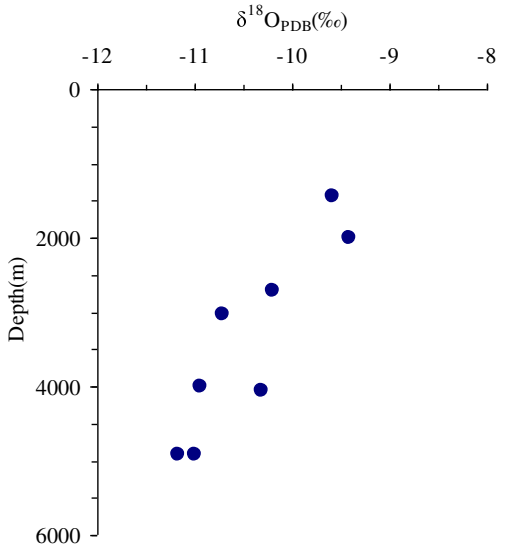

Fig. 9. The profile of $\delta^{18}O$ values along depths for the calcite cements in the Eboliang III-Yahu anticlines. The $\delta^{18}O$ values decrease steadily along depths.

precipitated directly from lakewater, because their lower $\delta^{18}O$ values indicate higher precipitating temperatures than those of the LC. Therefore, Group B calcites were likely precipitated during burial diagenetic stage from formation fluids within sedimentary strata, particularly within the LC. This, altogether with the distribution of well-developed fracture-abundant LC (Zeng et al., 2012) in the adjacent Yiliping sag (Table 1), supports a following scenario (Fig. 10): (i) pore water within the buried LC in the Yiliping sag was enriched in Ca^{2+}, HCO_3^- and CO_3^{2-}; (ii) such fluids were expelled from the LC and flowed rapidly upward to the shallower strata through the vertical faults; (iii) the partial pressure of carbon dioxide decreased, resulting in the precipitation of Group B calcites (Macdonald and North, 1974; Yan et al., 2009) in the sandstones.

5.1.3. Calcite cement formed directly from the paleo-lakewater

Point grain contacts in Sample 14 from the surface outcrop (Fig. 4A) indicate that the calcite cement formed when the detrital grains were relatively loose and thus before significant compaction. Moreover, the isotopic values of this calcite plots within the LC field (Fig. 8). This, altogether with its microcrystalline nature (Fig. 4A) indicates that the calcite was likely precipitated directly from the paleo-lakewater, probably due to evaporating concentration.

5.2. Relationship between calcite cements and hydrocarbon filling

Acidic fluids which contain carbon dioxide and carboxylic acid can be generated by thermocatalytic degradation of kerogen (Carothers and Kharaka, 1978; Dias et al., 2002; Means and Hubbard, 1987; Surdam and Crossey, 1989). Once such acidic fluids flow into reservoir rocks, they may dissolve feldspars, lithic fragments and existing carbonate cements, generating secondary porosity, authigenic quartz, and kaolinite (Surdam and Crossey, 1989). With consumption of organic acids due to water-rock reaction or thermal decarboxylation (Surdam and Crossey, 1989), diagenetic environment evolves from acidic to alkaline. Consequently, carbonate cements are precipitated alkaline pore water and occlude pores (Wang et al., 2007).

Kaolinite is stained by bitumen, indicating it predates hydrocarbon filling (Fig. 4G–H). The bitumen-stained kaolinite was partly dissolved, and the created space was subsequently occupied by Ca 1(Fig. 4G). These texture relationships suggest a diagenetic sequence of kaolinite → hydrocarbon filling → Ca 1, which corresponds to an acidic → hydrocarbon → alkaline fluid sequence. Two episodes of hydrocarbon filling (Hy 1, Hy 2) and two generations of calcite cement (Ca 1, Ca 2) from the same source indicate that this fluid sequence was likely repeated again in the same sandstone layer. Accordingly, the diagenetic sequence may be kaolinite → Hy 1 → Ca 1 → dissolution → Hy 2 → Ca 2.

In summary, the precipitation of Group A calcite cements is the result of evolution of source-rocks-derived fluids. Formation of calcite cements in Group B and outcrop, however, is not related to such fluids. Coincidentally, there is a good correlation between present exploration achievements and origins of calcite cements (Fig. 11): commercial oil

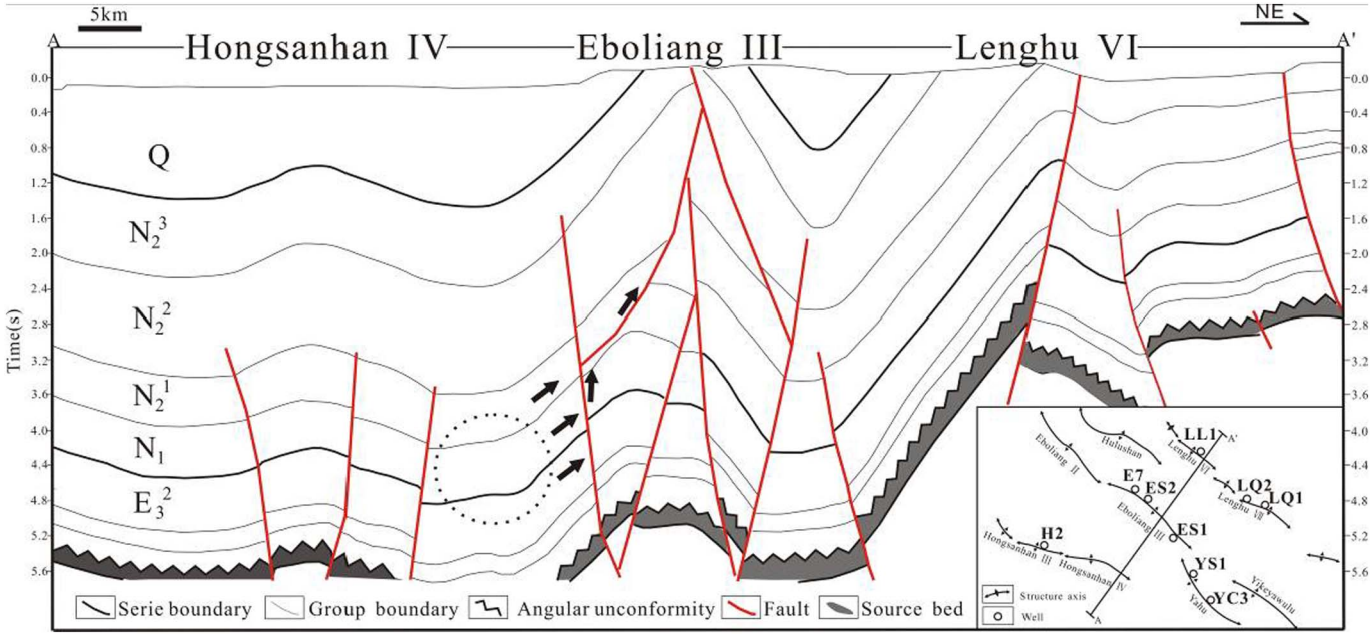

Fig. 10. Geological section crosscutting axes of Hongsanhan IV-Eboliang III-Lenghu VI anticlines in the central part of northern Qaidam Basin. Inorganic fluids from LC in the Yiliping sag flowed upward through faults and precipitated calcite cements within the sandstones in the Eboliang III-Yahu anticlines. Dotted circle marks the possible location of LC expelling the precipitating fluids. Black arrows indicate the possible pathways for the fluid flow.

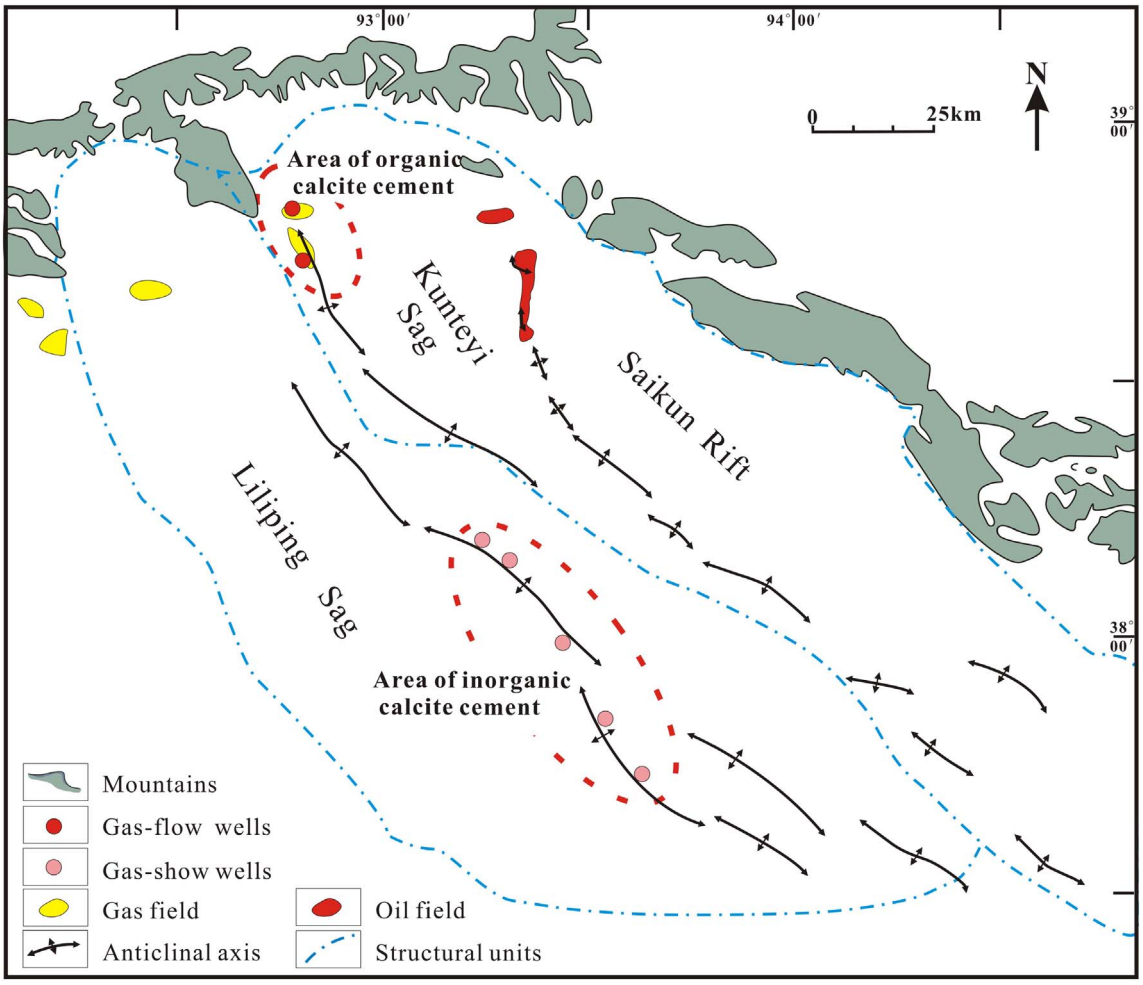

Fig. 11. Distribution of hydrocarbons, organic and inorganic calcite cements in the west section of the northern Qaidam Basin. Commercial oil and gas are only produced from areas with abundant organic calcite cements.

and gas are only produced from areas with abundant "*organic calcite cement*" (referring to a calcite cement that is enriched in carbon derived from an organic source). Based on this correlation, carbonate cements like Group A, can be regarded as indicators for hydrocarbon migration in the northern Qaidam Basin.

5.3. Impact on reservoir quality and hydrocarbon migration

Carbonate cements play an important role in controlling reservoir quality, which can further affect hydrocarbon migration (e.g., Esteban and Taberner, 2003; Heasley et al., 2000; Neilson and Oxtoby, 2008). The first episode of acidic fluid generated secondary pores and led to formation of kaolinite in the Jurassic reservoir sandstones of N1 well. Although the kaolinite was present in pores, the reservoir sandstones at that time should be permeable enough for hydrocarbon (Hy 1) migration, due to superposition of primary and secondary pores. Subsequently, Ca 1 occluded the pores, resulting in the highly calcite-cemented zones (e.g., Fig. 12A).

Despite absence of isotopic data, the residual calcite cements after dissolution (e.g., Figs. 4E, 12B) should correspond to Ca 1 based on the diagenetic sequence above. Thus, the dissolution-generated porous zones (Fig. 12) were cemented by Ca 1 before as well. Taking Ca 1 cementation in the shallow layer (i.e., Sample 1) into account, Ca 1 had probably occupied all the porosity in the sandstones of N1 well. However, the second episode of acidic fluid derived from the Jurassic source rocks partially dissolved the Ca 1-cemented reservoir, creating new porous zones (Fig. 12B) for subsequent migration and accumulation of the second generation of hydrocarbons (Hy 2). Finally, Ca 2 was precipitated from the alkaline pore water, generating the highly Ca 2-cemented zones (Fig. 12C).

The calcite cement in the outcrop (i.e. Sample 14) completely occluded the porosity in sandstones (Fig. 4A), providing little storage space for hydrocarbon even though hydrocarbon migration has occurred (Fig. 6D). In contrast to the Sample 14, other Group B calcite cements just only partially cemented the sandstones, keeping plenty of primary pores (Table 2; Fig. 4B). The reason that little hydrocarbons were produced from Group B calcite cemented sandstones maybe attributed to the lack of hydrocarbon migration.

In summary, the migration and accumulation of hydrocarbon in the Eboliang Anticline Belt was controlled by (1) hydrocarbon supply; and (2) dissolution of calcite-cemented reservoir sandstones. The secondary porous zones intercalated in calcite-cemented sandstones along the basin margin should be paid more attention in the next exploration.

5.4. Model of fluid flow and hydrocarbon migration

Bluish-white fluorescing oil inclusions (Fig. 6D) and LC-originated calcite cements both occurred in the Lower Youshashan formation (N_2^1y, Table 2). This indicates that Hy 2 and LC-derived fluids postdate the subsidence of N_2^1y. The timing of these fluids is expected to correspond to the late Neogene and early Quaternary, as the intense tectonic movements during that period caused uplift of mountains around the basin and development of decollement faults (Yin et al., 2008; Zeng, 2009), and probably induced fluid flow as well. The abnormal high

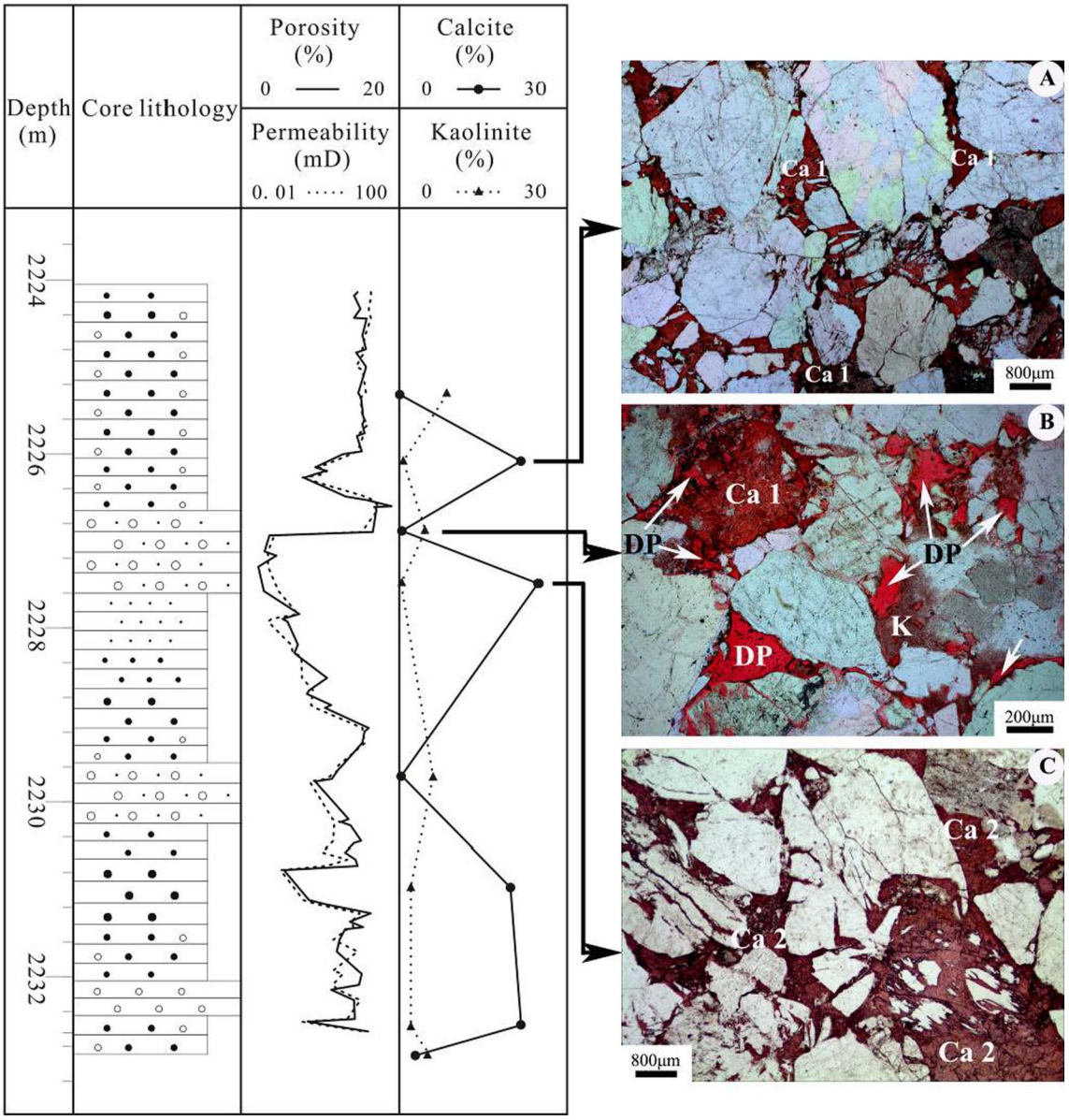

Fig. 12. Lithology, porosity, permeability, dissolution pore (DP) and calcite, kaolinite (K) contents of the sandstone reservoir in 2224–2233 m section of N1 well. The diagenetic sequence of Ca 1 cementation -partial dissolution –hydrocarbon accumulation- Ca 2 cementation resulted in alternate distribution of highly calcite-cemented zones and porous zones.

temperature of bluish-white fluorescing oil inclusions indicates rapid migration of Hy 2 through faults.

Based on events discussed above, as well as the tectonic-sedimentary evolution history of the basin (Yin et al., 2008; Zeng, 2009), we proposed a model of fluid flow and hydrocarbon migration in the northern Qaidam Basin (Fig. 13).

During the Cenozoic, LC was deposited in the areas lacking the sufficient supply of clastic sediments in the arid climate. Microcrystalline calcite (e.g., Sample 14) was precipitated from lake water due to evaporating concentration, and cemented in the intergranular pores of some loose sandy sediment along the lake margin (Fig. 13A). As the basin subsided continually, the Jurassic source rocks in the deeper strata gradually entered thermal degradation stage. The first episode of organic fluids including hydrocarbons from the source rocks flowed towards the basin margin through connected sandstone layers, resulting in an acidic → hydrocarbon → alkaline fluid evolution sequence identified in the reservoir sandstones. The acidic fluid generated secondary pores by dissolution of detritial grains and matrix and precipitated the kaolinite; the hydrocarbon migrated through the sandstones; and the alkaline fluid precipitated Group A calcites (excluding Ca 2) which generated highly calcite-cemented sandstones (process I in Fig. 13B).

Lateral compression during the late Neogene and early Quaternary resulted in strata deformation and in faults formation/reactivation. Various fluids across the basin were thus reactivated. In the central basin, the inorganic fluids derived from the buried strata of LC flowed rapidly upward through the vertical faults from the syncline into the sandstones in the anticlines. Group B calcites were precipitated from the fluids expelled from the LC and partially cemented the sandstones (Fig. 13C). More or less at the same stage, the second episode of organic fluids derived from the deep-seated Jurassic source rocks flowed through the faults towards the reservoir rocks along the basin margin (process II in Fig. 13B). This resulted in the same fluid evolution sequence as in the first episode. The partial dissolution of calcite cement (Ca 1) caused by the second episode of acidic fluid created new porous zones for subsequent hydrocarbon migration and accumulation. Finally, Ca 2 was precipitated and generated highly Ca 2-cemented zones.

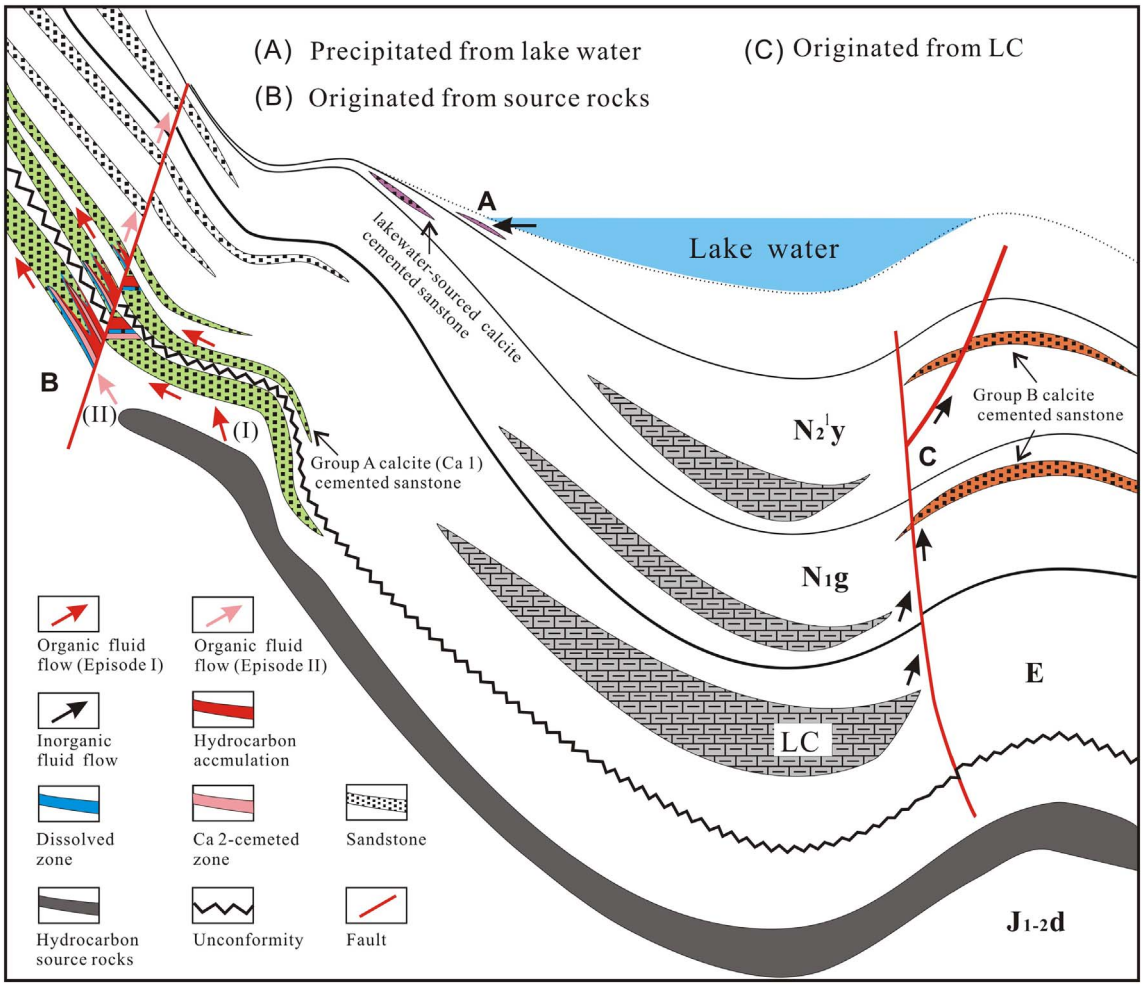

Fig. 13. Model of fluid flow and hydrocarbon migration in the northern Qaidam Basin.

6. Conclusions

Reconstructing fluid flow and hydrocarbon migration in continental basins is always challenging. In order to reveal fluid information within the continental Qaidam Basin (NW China), the diagenetic calcite cements in the reservoir sandstones were investigated using petrological and geochemical analysis. Important findings include:

(1) Calcite is the dominant cement in the sandstones, constituting up to 25% of rock volume. The $\delta^{13}C_{PDB}$ and $\delta^{18}O_{PDB}$ values of calcite cements display a wide isotopic range, varying from −13.5 to 2.5‰ and −16.7 to −4.7‰, respectively. Compared to the well-preserved lacustrine carbonates, the origins of diagenetic calcite cement were clearly identified, including (i) the Jurassic source rocks in thermal degradation stage, (ii) the lacustrine carbonates in the deeper strata, and (iii) the paleo-lakewater in the area.

(2) Dull-/bright-luminescence zones, two populations of fluid inclusion and two groups of isotopic values indicate two generations of calcite (Ca 1 and Ca 2) in the N1 well along the basin margin. Based on this, the petrographic observation suggests two episodes of organic fluid derived from the Jurassic source rocks, which resulted in two rounds of acidic → hydrocarbon → alkaline fluid evolution. The precipitation of Ca 1 generated highly calcite-cemented sandstones, which severely downgraded the reservoir quality. The new porous zones created by the second episode of acidic fluid provide secondary reservoir storage space for subsequent hydrocarbon accumulation, which should be paid more attention in next exploration.

(3) Pore-filling calcites from the central basin exhibit non/dull or bright CL without identifiable growth zones. Their $\delta^{13}C_{PDB}$ and $\delta^{18}O_{PDB}$ values are within a limited range (−4.2 to −2.0‰ and −11.2 to −9.4‰, respectively). The calcite cements were precipitated from the inorganic fluids derived from the lacustrine carbonates, which suggest a poor prospect for hydrocarbon migration, even though the cementation history did not occlude all porosity in the sandstones.

(4) Quantitative evaluation for the oxygen isotope fractionation caused by geothermal gradient suggests that the first episode of organic fluid flowed slowly through the connected sandstone layers towards the basin margin, while the LC-derived fluids in the central basin flowed upward rapidly along vertical faults. The second episode of aqueous and oil inclusions respectively homogenize at 120–150 °C and 82.8–128.5 °C, which are about 50 °C higher than the highest paleogeothermal temperatures experienced by the formations. This probably indicates that the main pathways for the second episode of organic fluid are faults as well.

(5) There is a good spatial correlation between the occurrence of ^{13}C-depleted calcite cements and the hydrocarbons. Thus, the ^{13}C-depleted calcite cement (relative to the lacustrine carbonates) may be used as an indicator of hydrocarbon migration in the northern Qaidam Basin.

Acknowledgements

We are grateful to Prof. Rui Sun for his suggestions on earlier versions of this manuscript, and to Drs. Shaofeng Dong, Zenghui Guo for their kind help in the micro-drilling sampling. We also thank Jian Zhao

and Wei Sha for their generous contribution of geological data for this study. This work was supported by the National Natural Science Foundation of China (No. 41402115), Opening Project (No. BJ08133-5) of the State Key Laboratory of Continental Dynamics.

References

Ankertell, J.M., Mriheel, I.Y., 2000. Depositional environment and diagensis of the Eocene Jdeir Formation, Gabes-Tripoli Basin, Western offshore, Libya. J. Pet. Geol. 23 (4), 425–447.

Baker, J.C., Kassan, J., Hamilton, P.J., 1995. Early diagenetic siderite as an indicator of depositional environment in the Triassic Rewan Group, southern Bowen Basin, eastern Australia. Sedimentology 43, 77–88.

Brigaud, B., Durlet, C., Deconinck, J., Vincent, B., Thierry, J., Trouiller, A., 2009. The origin and timing of multiphase cementation in carbonates: impact of regional scale geodynamic events on the Middle Jurassic limestone diagenesis (Paris Basin, France). Sediment. Geol. 222 (3–4), 161–180.

Calvo, R., Ayalon, A., Bein, A., Sass, E., 2011. Chemical and isotopic composition of diagenetic carbonate cements and its relation to hydrocarbon accumulation in the Heletz-Kokhav oil field (Israel). J. Geochem. Explor. 108 (1), 88–98.

Carothers, W.W., Kharaka, Y.K., 1978. Aliphatic acid anions in oil-field waters–implications for origin of natural gas. AAPG Bull. 62 (12), 2441–2453.

Chen, J., Shi, J., Sun, G., Wang, M., Ma, J., Zhou, K., Long, G., 2012. Diagenesis of lower-upper Youshashan formation and its impact on porosity in No. III structure of Eboliang area (in Chinese with English abstract). J. Lanzhou Univ. (Nat. Sci.) 48 (6), 1–7.

Chen, A., Zheng, M., Shi, L., Wang, H., Xu, J., 2017. Magnetostratigraphy of deep drilling core 15YZK01 in the northwestern Qaidam Basin (NE Tibetan Plateau): tectonic movement, salt deposits and their link to Quaternary glaciation. Quat. Int. 436, 201–211.

Deocampo, D.M., 2010. The geochemistry of continental carbonates. In: Alonso-Zarza, A.M., Tanner, L.H. (Eds.), Developments in Sedimentology, Chapter 1. Elsevier, pp. 1–59.

Dias, R.F., Freeman, K.H., Lewan, M.D., Franks, S.G., 2002. $\delta^{13}C$ of low-molecular-weight organic acids generated by the hydrous pyrolysis of oil-prone source rocks. Geochim. Cosmochim. Acta 66 (15), 2755–2769.

Dutton, S.P., Land, L.S., 1985. Meteoric burial diagenesis of Pennsylvanian arkosic sandstones, southwestern Anadarko Basin, Texas. AAPG Bull. 69, 22–38.

El-Ghali, M.A.K., El Khoriby, E., Mansurbeg, H., Morad, S., Ogle, N., 2013. Distribution of carbonate cements within depositional facies and sequence stratigraphic framework of shoreface and deltaic arenites, Lower Miocene, the Gulf of Suez rift, Egypt. Mar. Pet. Geol. 45 (4), 267–280.

Esteban, M., Taberner, C., 2003. Secondary porosity development during late burial in carbonate reservoirs as a result of mixing and/or cooling of brines. J. Geochem. Explor. 78-79, 355–359.

Fan, Q., Ma, H., Wei, H., Shan, F., An, F., Xu, L., Madsen, D.B., 2014. Late Pleistocene paleoclimatic history documented by an oxygen isotope record from carbonate sediments in Qarhan Salt Lake, NE Qinghai-Tibetan Plateau. J. Asian Earth Sci. 85, 202–209.

Fan, C., Wang, Z., Wang, A., Fu, S., Wang, L., Zhang, Y., Kong, H., Zhang, X., 2016. Identification and calculation of transfer overpressure in the northern Qaidam Basin, northwest China. AAPG Bull. 100 (1), 23–39.

Folk, R.L., 1980. Petrology of Sedimentary Rocks. Hemphill Publishing Co., Austin, Texas.

Fouke, B.W., Rakovan, J., 2001. An integrated cathodoluminescence videocapture microsampling system. J. Sediment. Res. 71, 509–513.

Graham, S.A., Chamberlain, C.P., Yue, Y., Ritts, B.D., Hanson, A.D., Horton, T.W., Waldbauer, J.R., Poage, M.A., Feng, X., 2005. Stable isotope records of Cenozoic climate and topography, Tibetan Plateau and Tarim Basin. Am. J. Sci. 305 (2), 101–118.

Guo, K., Zeng, J., Li, Y., Liu, T., 2013. Geochemical characteristics of tectonic fracture-filling calcite in Yanchang formation of Longdong area and its relationship with hydrocarbon fluid flow (in Chinese with English abstract). J. China Univ. Pet. (Nat. Sci. Ed.) 37 (2), 36–49.

Heasley, E.C., Worden, R.H., Hendry, J.P., 2000. Cement distribution in a carbonate reservoir: recognition of a palaeo oil–water contact and its relationship to reservoir quality in the Humbly Grove field, onshore, UK. Mar. Pet. Geol. 17 (5), 639–654.

Heermance, R.V., Pullen, A., Kapp, P., Garzione, C.N., Bogue, S., Ding, L., Song, P., Song, P., 2013. Climatic and tectonic controls on sedimentation and erosion during the Pliocene-Quaternary in the Qaidam Basin (China). GSA Bull. 125 (5/6), 833–856.

Huang, C., Zhao, F., Yuan, J., Wu, L., 2016. The characteristics of dolomite reservoir in saline lacustrine Basin, Qaidam, China. Carbonates Evaporites 31 (3), 307–317.

Irwin, H., Curtis, C., Coleman, M., 1977. Isotopic evidence for source of diagenetic carbonates formed during burial of organic-rich sediments. Nature 269 (5625), 209–213.

Jian, X., Guan, P., Zhang, D., Zhang, W., Feng, F., Liu, R., Lin, S., 2013. Provenance of Tertiary sandstone in the northern Qaidam basin, northeastern Tibetan Plateau: Integration of framework petrography, heavy mineral analysis and mineral chemistry. Sediment. Geol. 290, 109–125.

Jian, X., Guan, P., Fu, S., Zhang, D., Zhang, W., Zhang, Y., 2014. Miocene sedimentary environment and climate change in the northwestern Qaidam basin, northeastern Tibetan Plateau: facies, biomarker and stable isotopic evidences. Palaeogeogr. Palaeoclimatol. Palaeoecol. 414, 320–331.

Kent-Corson, M.L., Ritts, B.D., Zhuang, G., Bovet, P.M., Graham, S.A., Chamberlain, C.P., 2009. Stable isotopic constraints on the tectonic, topographic, and climatic evolution of the northern margin of the Tibetan Plateau. Earth Planet. Sci. Lett. 282 (1–4), 158–166.

Li, F., Meng, L., Fang, Z., Li, L., Lin, H., 2012. Palaeogeographic evolution of the Paleogene and Neogene in north margin of Qaidam Basin (in Chinese with English abstract). J. Palaeogeogr. 14 (05), 596–606.

Liu, Z., Wang, Y., Chen, Y., Li, X., Li, Q., 1998. Magnetostratigraphy and sedimentologically derived geochronology of the Quaternary lacustrine deposits of a 3000 m thick sequence in the central Qaidam basin, western China. Palaeogeogr. Palaeoclimatol. Palaeoecol. 140 (1–4), 459–473.

Luo, X., Sun, Y., Wang, L., Xiao, A., Ma, L., Zhang, X., Wang, Z., Song, C., 2013. Dynamics of hydrocarbon accumulation in the west section of the northern margin of the Qaidam Basin, NW China. Pet. Explor. Dev. 40 (2), 159–170.

Macdonald, R.W., North, N.A., 1974. The effect of pressure on the solubility of $CaCO_3$, CaF_2, and $SrSO_4$ in water. Can. J. Chem. 52 (52), 3181–3186.

Maliva, R.G., 1995. Recurrent neomorphic and cement microtextures from different diagenetic environments, Quaternary to Late Neogene carbonates, Great Bahama bank. Sediment. Geol. 97 (1–2), 1–7.

Mansour, A.S., Rifai, R.I., Shaaban, M.N., 2014. Geochemical constraint on the origin of the multi-mineralogic carbonate cements in the subsurface Middle Jurassic sandstones, Central Sinai, Egypt. J. Geochem. Explor. 143 (3), 163–173.

Mansurbeg, H., De Ros, L.F., Morad, S., Ketzer, J.M., El-Ghali, M.A.K., Caja, M.A., Othman, R., 2012. Meteoric-water diagenesis in late Cretaceous canyon-fill turbidite reservoirs from the Espírito Santo Basin, eastern Brazil. Mar. Pet. Geol. 37 (1), 7–26.

McCrea, J.M., 1950. On the isotopic chemistry of carbonates and a paleotemperature scale. J. Chem. Phys. 18 (6), 849–857.

Means, J.L., Hubbard, N., 1987. Short-chain aliphatic acid anions in deep subsurface brines: a review of their origin, occurrence, properties, and importance and new data on their distribution and geochemical implications in the Palo Duro Basin, Texas. Org. Geochem. 11 (3), 177–191.

Morad, S., Ketzer, J.M., De Ros, L.F., 2000. Spatial and temporal distribution of diagenetic alterations in siliciclastic rocks: implications for mass transfer in sedimentary basins. Sedimentology 47, 95–120.

Morad, S., De, Ros, Al-Aasm, L.F., I.S., 1996. Origin of low $\delta^{18}O$, pre-compactional ferroan carbonates in the marine Stø Formation (Middle Jurassic), offshore NW Norway. Mar. Pet. Geol. 13 (2), 263–276.

Mozley, P.S., Hoernle, K., 1990. Geochemistry of carbonate cements in the Sag River and Shublik Formations (Triassic/Jurassic), North Slope, Alaska: implications for the geochemical evolution of formation waters. Sedimentology 37 (5), 817–836.

Mozley, P.S., Wersin, P., 1992. Isotopic composition of siderite as an indicator of depositional environment. Geology 20, 817–820.

Munz, I.A., 2001. Petroleum inclusions in sedimentary basins: systematics, analytical methods and applications. Lithos 55 (1–4), 195–212.

Neilson, J.E., Oxtoby, N.H., 2008. The relationship between petroleum, exotic cements and reservoir quality in carbonates – a review. Mar. Pet. Geol. 25 (8), 778–790.

Odigi, M.I., Amajor, L.C., 2010. Geochemistry of carbonate cements in Cretaceous sandstones, southeast Benue Trough, Nigeria: implications for geochemical evolution of formation waters. J. Afr. Earth Sci. 57 (3), 213–226.

O'Neil, J.R., Clayton, R.N., Mayeda, T.K., 1969. Oxygen isotope fractionation in divalent metal carbonate. J. Chem. Phys. 51 (12), 5547–5558.

Qing, H., Chi, G., Zhang, S., 2006. Origin of coarse-crystalline calcite cement in Early Ordovician carbonate rocks, Ordos basin, northern China: Insights from oxygen and carbon isotopes and fluid inclusion microthermometry. J. Geochem. Explor. 89 (1–3), 344–347.

Qiu, N., 2002. Tectono-thermal evolution of the Qaidam Basin, China: evidence from Ro and apatite fission track data. Pet. Geosci. 8 (3), 279–285.

Rieser, A.B., Neubauer, F., Liu, Y., Ge, X., 2005. Sandstone provenance of north-western sectors of the intracontinental Cenozoic Qaidam basin, western China: tectonic vs. climatic control. Sediment. Geol. 177 (1), 1–18.

Rieser, A.B., Bojar, A.V., Neubauer, F., Genser, J., Liu, Y., Ge, X.H., Friedl, G., 2009. Monitoring Cenozoic climate evolution of northeastern Tibet: stable isotope constraints from the western Qaidam Basin, China. Int. J. Earth Sci. 98 (5), 1063–1075.

Ritts, B.D., 1999. Lower-Middle Jurassic nonmarine source rocks and petroleum systems of the northern Qaidam basin, northwest China. AAPG Bull. 83 (12), 1980–2005.

Stasiuk, L.D., Snowdon, L.R., 1997. Fluorescence micro-spectrometry of synthetic and natural hydrocarbon fluid inclusions: crude oil chemistry, density and application to petroleum migration. Appl. Geochem. 12 (3), 229–241.

Sun, Z., Sun, Z., Lu, H., Yin, X., 2010. Characteristics of carbonate cements in sandstone reservoirs: a case from Yanchang Formation, middle and southern Ordos Basin, China. Pet. Explor. Dev. 37 (5), 543–551.

Sun, G., Wang, H., Zhou, K., Wang, W., Zhou, G., Mang, J., Chen, Z., 2014. Characteristics and significance of carbon and oxygen isotopic compositions of carbonate cements in Jiulongshan region, northern edge of Qaidam Basin (In Chinese with English abstract). Nat. Gas Geosci. 25 (09), 1358–1365.

Surdam, R.C., Crossey, L., 1989. Organic-inorganic interactions and sandstone diagenesis. AAPG Bull. 73, 1–23.

Teichert, B.M.A., Johnson, J.E., Solomon, E.A., Giosan, L., Rose, K., Kocherla, M., Connolly, E.C., Torres, M.E., 2014. Composition and origin of authigenic carbonates in the Krishna-Godavari and Mahanadi Basins, eastern continental margin of India. Mar. Pet. Geol. 58, 438–460.

Wang, D., 2000. Stable Isotopic Geochemistry of Petroleum (in Chinese). Petroleum Industry Press, Beijing.

Wang, F., Wang, B., 2006. Diagenesis of reservoir rocks of the lower Jurassic and its influence on porosity modification in north Qaidam Basin (in Chinese with English abstract). J. Lanzhou Univ. (Nat. Sci.) 42 (05), 1–6.

Wang, D., Zhang, Y., 2001. A study on the origin of the carbonate cements within reservoirs in the external metamorphic belt of the Bohai Bay oil-gas bearing region (in

Chinese with English abstract). Pet. Explor. Dev. 28 (2), 40–42.
Wang, Q., Zhuo, X., Chen, G., Li, X., 2007. Characteristics of carbon and oxygen isotopic compositions of carbonate cements in Triassic Yanchang sandstone in Ordos Basin (in Chinese with English abstract). Nat. Gas Ind. 27 (10), 28–32.
Wang, Q., Bai, B., Li, X., Chen, G., Zhuo, X., Zhang, R., 2008. Diagnetic evolution characteristics of deeply-buried clastic reservoirs, northern Qaidam Basin: a case study from Well Kun 2 (in Chinese with English abstract). Nat. Gas Geosci. 19 (02), 157–164.
Wang, T., Yang, S., Duan, S., Chen, H., Liu, H., Cao, J., 2015. Multi-stage primary and secondary hydrocarbon migration and accumulation in lacustrine Jurassic petroleum systems in the northern Qaidam Basin, NW China. Mar. Pet. Geol. 62, 90–101.
Wang, J., Cao, Y., Liu, K., Liu, J., Xue, X., Xu, Q., 2016. Pore fluid evolution, distribution and water-rock interactions of carbonate cements in red-bed sandstone reservoirs in the Dongying Depression, China. Mar. Pet. Geol. 72, 279–294.
Xia, W., Zhang, N., Yuan, X., Fan, L., Zhang, B., 2001. Cenozoic Qaidam Basin, China: a stronger tectonic inversed, extensional rifted basin. AAPG Bull. 85 (4), 715–736.
Xiong, D., Azmy, K., Blamey, N.J.F., 2016. Diagenesis and origin of calcite cement in the Flemish Pass Basin sandstone reservoir (Upper Jurassic): implications for porosity development. Mar. Pet. Geol. 70, 93–118.
Yan, Z., Liu, H., Zhang, Z., 2009. Effect of temperature and Pco_2 on the solubility of calcite and dolomite (in Chinese with English abstract). Carslogica Sinica 28 (1), 7–10.
Yang, Y., Zhang, B., Zhao, C., Xu, T., 2004. Mesozoic source rocks and petroleum systems of the northeastern Qaidam basin, northwest China. AAPG Bull. 88 (1), 115–125.
Yin, A., Harrison, T.M., 2003. Geologic evolution of the Himalayan-Tibetan Orogen. Annu. Rev. Earth Planet. Sci. 28 (28), 211–280.
Yin, C., Li, W., Andrea, R., Liu, Y., Chen, Y., Gong, Q., 2007. Cenozoic climate changes in the Qaidam Basin, western China: evidenced from carbon and oxygen stable isotope (in Chinese with English abstract). J. Jilin Univ. (Earth Sci. Ed.) 37 (5), 901–907.
Yin, A., Dang, Y., Wang, L., Jiang, W., Zhou, S., Chen, X., Gehrels, G.E., McRivette, M.W., 2008. Cenozoic tectonic evolution of Qaidam Basin and its surrounding regions (Part 1): the southern Qilian Shan-Nan Shan thrust belt and northern Qaidam Basin. GSA Bull. 120 (7/8), 813–846.
Yuan, J., Huang, C., Zhao, F., Pan, X., 2015. Carbon and oxygen isotopic compositions, and palaeoenvironmental significance of saline lacustrine dolomite from the Qaidam Basin, Western China. J. Pet. Sci. Eng. 135, 596–607.
Zeng, C., 2009. Jurassic Tectonic Evolution and Its Control Over Hydrocarbon Accumulation in the North Margin of Qaidam Basin (in Chinese with English Abstract) (Ph.D. Thesis). China University of Mining and Technology, Xuzhou, China.
Zeng, L., Tang, X., Wang, T., Gong, L., 2012. The influence of fracture cements in tight Paleogene saline lacustrine carbonate reservoirs, western Qaidam Basin, northwest China. AAPG Bull. 96 (11), 2003–2017.
Zhai, D., Xiao, J., Zhou, L., Wen, R., Chang, Z., Wang, X., Jin, X., Pang, Q., Itoh, S., 2011. Holocene East Asian monsoon variation inferred from species assemblage and shell chemistry of the ostracodes from Hulun Lake, Inner Mongolia. Quat. Res. 75 (3), 512–522.
Zhang, Y., 2010. Diagenesis Research on the Cenozonic Reservoir Sandstones in the West Part of Northern Margin of Qaidam Basin (in Chinese With English Abstract) (M.S. Thesis). Chengdu University of Technology, Chengdu, China.
Zhang, M., Yin, M., Zhou, J., Chen, S., Zhang, Y., 2004. Sedimentary facies of carbonate rocks in the Paleogene and Neogene in western Qaidam Basin (in Chinese with English abstract). J. Palaeogeogr. 6 (4), 391–400.
Zhao, F., 2015. Lacustrine algal limestone reservoir in western Qaidam Basin, China. Carbonates Evaporites 30 (2), 127–133.
Zhu, L., Wang, C., Zheng, H., Xiang, F., Yi, H., Liu, D., 2006. Tectonic and sedimentary evolution of basins in the northeast of Qinghai-Tibet Plateau and their implication for the northward growth of the Plateau. Palaeogeogr. Palaeoclimatol. Palaeoecol. 241 (1), 49–60.